VIP Proteins Very Important Paper

How to cite: *Angew. Chem. Int. Ed.* **2021**, *60*, 25346–25355
International Edition: doi.org/10.1002/anie.202108961
German Edition: doi.org/10.1002/ange.202108961

APEX2-based Proximity Labeling of Atox1 Identifies CRIP2 as a Nuclear Copper-binding Protein that Regulates Autophagy Activation

*Lin Chen[+], Na Li[+], Meiqi Zhang[+], Mingming Sun, Jiaxuan Bian, Bo Yang, Zhengcunxiao Li, Jiayu Wang, Fei Li, Xiaomeng Shi, Yuan Wang, Feng Yuan, Peng Zou, Changliang Shan, and Jing Wang**

Abstract: *Mammalian cell nuclei contain copper, and cancer cells are known to accumulate aberrantly high copper levels, yet the mechanisms underlying nuclear accumulation and copper's broader functional significance remain poorly understood. Here, by combining APEX2-based proximity labeling focused on the copper chaperone Atox1 with mass spectrometry we identified a previously unrecognized nuclear copper binding protein, Cysteine-rich protein 2 (CRIP2), that interacts with Atox1 in the nucleus. We show that Atox1 transfers copper to CRIP2, which induces a change in CRIP2's secondary structure that ultimately promotes its ubiquitin-mediated proteasomal degradation. Finally, we demonstrate that depletion of CRIP2-as well as copper-induced CRIP2 degradation-elevates ROS levels and activates autophagy in H1299 cells. Thus, our study establishes that CRIP2 as an autophagic suppressor protein and implicates CRIP2-mediated copper metabolism in the activation of autophagy in cancer cells.*

Introduction

Copper is an essential metal ion with many demonstrated biological functions.[1] It can interfere with proteins containing iron-sulfur clusters and can displace other metals such as zinc from metalloproteins, thereby inhibiting their activity.[2] Tumors are known to have high metabolic demand for copper,[3] but the reason is unclear. Previous studies have demonstrated that modulation of copper levels can regulate MAPK signaling, lipid metabolism, and autophagy,[4] in addition to affecting tumor angiogenesis, procession, and metastasis.[5] In the context of cancer, elevated copper levels in both cancer tissues and cancer patient sera may support the multi-stage acquisition of tumorigenic properties, potentially by functioning as a structural or catalytic cofactor for specific proteins with functions in cancer initiation and/or progression.[6] Thus, organisms have evolved sophisticated mechanisms to strictly regulate both copper levels and the delivery of copper to copper-requiring proteins.

The human copper chaperone Atox1 delivers copper to P1B type ATPases in the Golgi network, for incorporation into essential Cu-dependent enzymes.[7] A handful of previous studies have implied that Atox1 mediates breast cancer cell migration via coordinated copper transport through the ATP7A-LOX axis.[8] It is also known that Atox1 can translocate to the nucleus where it binds with cell cycle proteins (e.g., cyclin D1) and perhaps functions as a transcription factor (TF) to promote cell proliferation.[9] However, the copper species that is brought into and retained in the nucleus, and the proteins that may coordinate copper activities are not well defined. Thus, it would be informative to determine the form of copper which enters (and is retained) in nuclei of cancer cells, and a deeper understanding of Atox1's interaction partners and regulatory functions could help decipher how copper metabolism impacts cancer. Many studies have demonstrated that Atox1 delivers copper to downstream copper-binding proteins via weak, dynamic protein-protein interactions.[10] However, the analytical methods used to date for profiling Atox1 interactions (e.g., bioinformatics method and yeast two-hybrid screening) capture only the most stable interaction partners,[11] thus likely missing highly transient and/or weaker Atox1 interaction proteins.

In this context, we describe here the integration of APEX2-based proximity labeling in combination with high resolution quantitative mass spectrometry to determine the interaction partners of Atox1 in the nucleus of lung cancer H1299 cells. APEX2 can be fused to a target protein, followed by treatment with biotin-phenol (BP) and H_2O_2. Upon activation by H_2O_2, APEX2 catalyzes the formation of short lived (<1 ms) and small labeling radius (<20 nm) biotin-phenoxyl radicals, which covalently conjugate with electron-rich amino acid residues of nearby proteins.[12] Using this

[*] L. Chen,[+] N. Li,[+] M. Q. Zhang,[+] J. X. Bian, B. Yang, Z. C. Li, J. Y. Wang, F. Li, X. M. Shi, Y. Wang, Prof. J. Wang
State Key Laboratory of Natural and Biomimetic Drugs
Department of Chemical Biology, School of Pharmaceutical Sciences
Peking University, Beijing 100191 (China)
E-mail: wangjingsioc@pku.edu.cn

M. M. Sun, C. L. Shan
State Key Laboratory of Medicinal Chemical Biology
College of Pharmacy, Nankai University
Tianjin 300071 (China)

F. Yuan, P. Zou
College of Chemistry and Molecular Engineering, Synthetic and Functional Biomolecules Center, Beijing National Laboratory for Molecular Sciences, Key Laboratory of Bioorganic Chemistry and Molecular Engineering of Ministry of Education, Peking University
Beijing 100871 (China)

[+] These authors contributed equally to this work.

Supporting information and the ORCID identification number(s) for the author(s) of this article can be found under: https://doi.org/10.1002/anie.202108961.

strategy, we identified a previously unrecognized interaction between Atox1 and the nucleus-localized, copper-binding protein Cysteine-rich protein 2 (CRIP2). Finally, we demonstrate that Atox1 binds to and facilities copper loading into CRIP2, thereby promoting its ubiquitin-mediated degradation and inducing autophagy.

Results and Discussion

Previous studies have reported that Atox1 is localized primarily in the cytosol, although there are also studies reporting its nuclear localization.[13] We conducted immunofluorescence staining to monitor Atox1 localization in lung cancer H1299 cells and confirmed that Atox1 was present in both the cytosol and the nucleus (Figure S1A). We then generated a fusion construct comprising Atox1 with a C-terminal nuclear localization sequence (NLS)-tag and a N-terminal Flag-tag, and observed the expected co-localization of Atox1-NLS and nuclear marker DAPI by immunofluorescence staining (Figure S1B). Subsequently, inductively coupled plasma mass spectrometry (ICP-MS) showed that the overexpression of this Atox1-NLS fusion protein resulted in elevated nuclear copper content (Figure S1C and S1D). These results suggest that the copper chaperone protein Atox1 can deliver copper into the nucleus. Note that the nuclear concentration of over-expressed Atox1 in these cells may exceed normal physiological levels.

Next, we employed an APEX2-based proximity labeling strategy to identify proteins that interact with Atox1 in the nucleus of H1299 cells (Figure 1 A). To this end, we genetically fused APEX2 with our C-terminal NLS-tagged Atox1

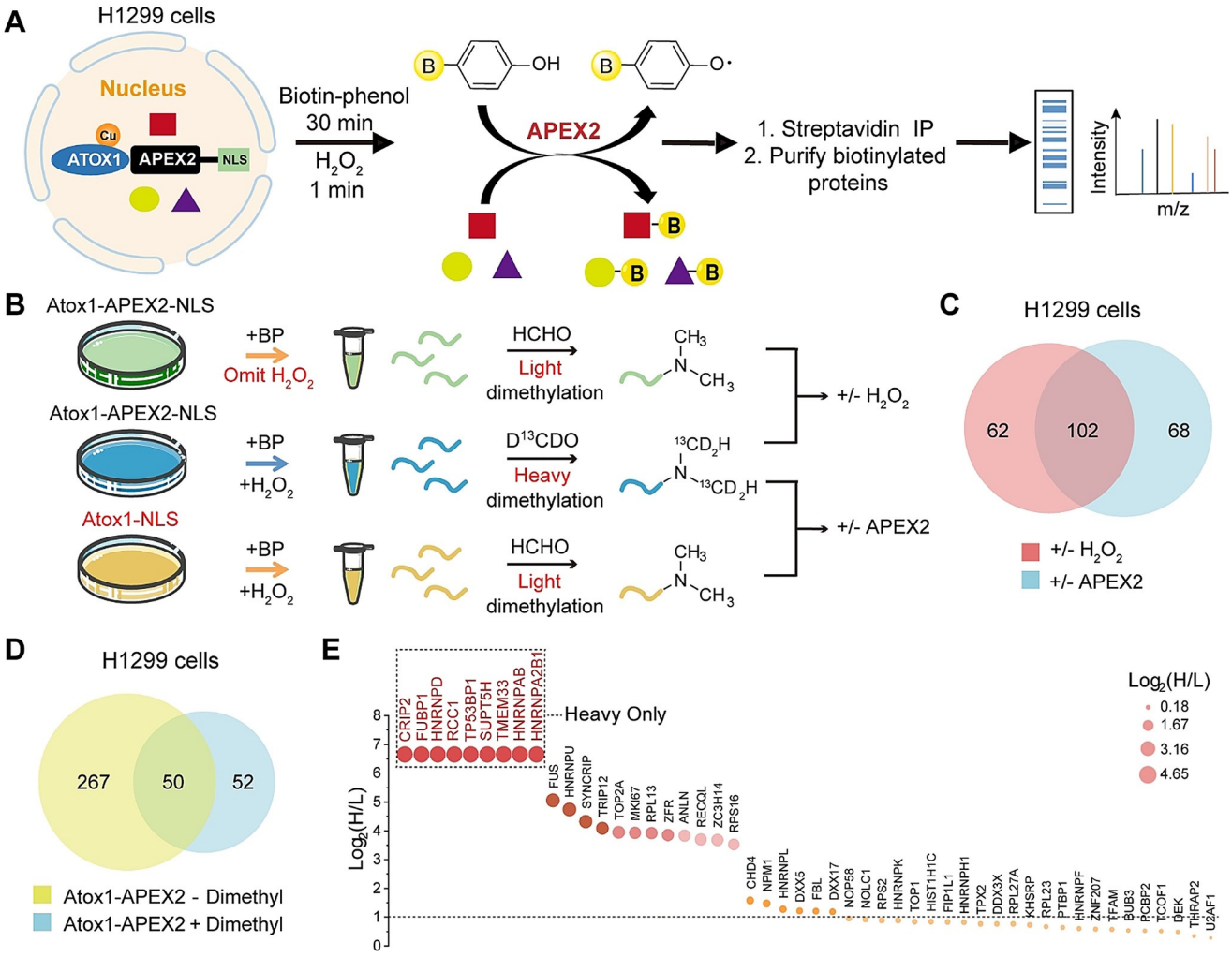

Figure 1. Proteomics analysis of Atox1-interacting proteins in the nucleus of H1299 cells using APEX2-based proximity labeling. A) Schematic overview of APEX2-catalyzed biotinylation in the nucleus. B) Illustration depicting the strategy to identify Atox1 interaction partners in H1299 cells by quantitative MS-based proteomics. Experimental workflow for the preparation of samples for analysis. We established "heavy" and "light" samples using the dimethyl labeling. The "heavy" samples were labeled by pre-loading BP for 30 min, then adding 1 mM H_2O_2 for 1 min to initiate biotinylation. Two "light" sample were processed in parallel as negative controls, one with APEX omitted (−APEX2), and one with H_2O_2 omitted ($-H_2O_2$). C) Venn diagrams showing the numbers of proteins identified across two proteomics datasets ($+/-H_2O_2$ and +/−APEX2) of dimethyl labeling. D) Venn diagram illustrating the overlapping protein numbers between the APEX2-Atox1 without dimethyl (−Dimethyl) and APEX2-Atox1 with dimethyl (+Dimethyl) labeling. E) The rank plot of 50 most highly enriched proteins, according to the ranking of H/L ratios, including 9 proteins which were only detected in the heavy sample.

and confirmed that this fusion construct localized to the nucleus (Figure S2A). Then, to examine the biotinylation activity of the Atox1-APEX2 fusion construct, we characterized the recombinant fusion protein by fluorescence imaging. Following treatment with H_2O_2 for 1 min in the presence of biotin-phenol, cells were fixed, permeabilized, and stained with AlexaFluor488-conjugated streptavidin (AF488-streptavidin) for visualization of the biotinylation signal. Fluorescence imaging showed that the AF488-streptavidin signal overlapped with the nuclear marker DAPI (Figure S2B). No biotinylation signal was observed in the negative control (i.e., samples from which the H_2O_2 treatment was omitted). Thus, the Atox1-APEX2 fusion protein can target the nucleus and is able to biotinylate proteins contained within the nucleus.

To help minimize false positives, we also examined samples that omitted the H_2O_2 treatment (-H_2O_2) and cells expressing the Atox1-NLS construct (i.e., lacking the APEX2 fusion: -APEX2) as negative controls. Non-nuclear proteins were removed by subcellular fractionation, and nuclear biotinylated proteins were enriched using streptavidin beads, followed by immunoblotting and silver staining. Atox1-APEX2-NLS-expressing cells treated with H_2O_2 yielded many recovered biotinylated proteins; two negative control cells (-H_2O_2 and -APEX2) yielded far fewer proteins (Figure S3A). In total, 412 unique proteins were detected in the Atox1-APEX2-NLS group. After filtering two negative control cells (-H_2O_2 and -APEX2), 317 remaining proteins were identified as being in close proximity to Atox1 in the nucleus (Figure S3B). Among them, DNMT1 has been reported as an Atox1 interaction partner,[11a] supporting the success of our APEX2 proximity labeling strategy.

Stable isotope dimethyl labeling is a chemical labeling strategy to quantitatively measure protein abundance between samples.[14] We subjected H1299 cells to proximity labeling followed by dimethyl labeling using CH_2O or $^{13}CD_2O$ (Figure 1B). A total of 172 and 207 possible Atox1-interacting proteins were identified in MS analyses of two biological experiments: +/- H_2O_2 and +/- APEX2. The proteomics data were filtered with the heavy to light (H/L) ratio beyond 1 for +/- APEX2 and +/- H_2O_2 experiments, leading to the enrichment of 164 and 170 proteins, respectively (Figures 1C). Intersecting these two datasets yielded a list of 102 overlapping proteins. Given the still large number of potential candidates, we performed one last enrichment step: by comparing the APEX2-labeled proteins with dimethyl-labeled proteins, we further narrowed our list to 50 proteins, including 9 proteins (CRIP2, FUBP1, HNRNPD, RCC1, TP53BP1, SUPT5H, TMEM33, HNRNPAB, and HNRNPA2B1) which were only detected in the heavy sample (Figure 1D and Table S1).

Since the copper-binding motifs of CXXC and CXXXC are commonly observed in metal binding proteins (e.g., Atox1),[15] we checked the amino acid sequences of the 9 proteins for CXXC features (Figure S4). Although cysteine was widely present in the 9 proteins, a CXXC feature was only found in the LIM domain of Cysteine-rich protein 2 (CRIP2) (Figure S4). We next searched an NMR-resolved structure for CRIP2 from the RCSB protein data bank (PDB: 2CU8), which indicated that this protein has two LIM domains, each having double zinc finger (ZF)-like structures containing two zinc ions[16] (Figure 2A). Of note, zinc has been reported a metal cofactor for CRIP2.[17] However, the presence of CXXC feature within ZF motifs likely allows the ZF to coordinate with other metal ions-such as Cu^I-implying that CRIP2 could be a copper-binding protein. The ability of Cu^I to displace Zn^{II} from ZF, thereby altering the ZF stability and function, could alter its function.[18] Previous studies have shown that CRIP2 participates in cardiovascular development, tumorigenesis, angiogenesis, migration, and apoptosis.[19] However, the stoichiometry of copper binding to CRIP2, and whether copper substitution CRIP2 regulates zinc finger domains function remain largely unknown.

To confirm the interaction between Atox1 and CRIP2, we initially confirmed the co-localization of Atox1 and CRIP2 in the nucleus by immunofluorescence staining (Figure 2B). Next, we co-transfected an Atox1-APEX2-NLS construct and a Myc-tagged CRIP2 fusion into H1299 cells, followed by treatment with H_2O_2 for 1 min in the presence of biotin-phenol. We then purified the lysates using streptavidin beads and detected that CRIP2 was enriched in the Atox1-APEX2 streptavidin pull-down sample (Figure 2C), supporting that Atox1 interacts with CRIP2. Additionally, surface plasmon resonance (SPR) analysis of recombinant Atox1 and CRIP2 confirmed that there was a direct interaction between these two proteins (Figure S5). The binding affinity between Atox1 and CRIP2 (Cu^I-free state) was 6.11×10^{-7} M and was 1.51×10^{-8} M in the presence of Cu^I, results indicating that Cu^I can further promote the interaction between Atox1 and CRIP2 (Figure 2D). Taken together, these data strongly suggest that Atox1 directly interacts with CRIP2.

To delineate the impact of cysteine residues on CRIP2′s apparent interaction with copper, we mutated 12 cysteine residues to serine to eliminate copper binding ability, thus generating a CRIP2 copper-binding mutant (CBM) that we termed "$CRIP2^{CBM}$" (Figure S6A). Free-thiol quantification upon reaction with 5,5′-dithiobis-(2-nitrobenzoic acid) (DTNB) yielded the expected number of accessible Cys residues for the $CRIP2^{WT}$ and $CRIP2^{CBM}$ proteins (Figure S6B and S6C). To test whether CRIP2 functions as a copper-binding protein, we used ICP-MS to quantify the copper-binding capacities of these two proteins. Upon pre-incubation with copper, we found that the copper concentration of the $CRIP2^{WT}$ protein sample was significantly elevated compared to the $CRIP2^{CBM}$ sample, supporting that CRIP2 is indeed a copper binding protein (Figure 3A).

We next confirmed the copper binding of CRIP2 by monitoring spectral changes in the near-UV circular dichroism (CD) region (250–320 nm), which is dominated by ligand-to-metal charge transfer from Cys-S to Cu.[20] Briefly, Cu^I solutions prepared in argon-degassed 20% CH_3CN were stable in all experiments (Figure S6D). Cu^I addition to CRIP2 resulted in distinct near-UV CD changes in accord with copper binding (Figure S6E). Then, to test whether CRIP2 binds copper in cells, we incubated the proteins from CRIP2 overexpression cells with GSH beads preloaded with copper or zinc: CRIP2 binds with a copper-charged resin and with

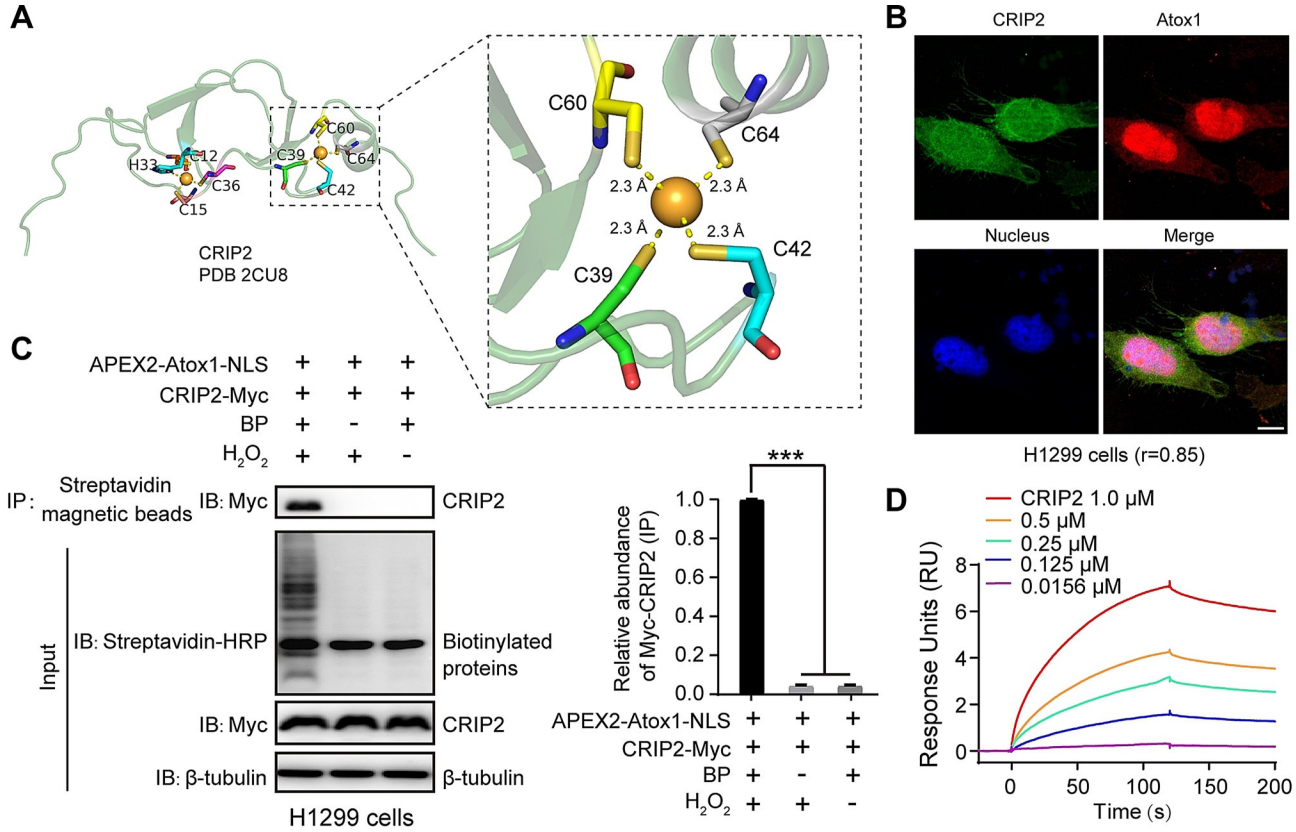

Figure 2. Verification of the Atox1-CRIP2 interaction. A) NMR-resolved structure of the CRIP2 LIM1 domain (PDB: 2CU8). Zn^{II} are shown as orange spheres, and the coordinating cysteine and histidine residues are shown as sticks. B) Immunofluorescence detection of Atox1-NLS (red) and CRIP2 (green) co-localization in H1299 cells using antibodies against Atox1 and CRIP2. The Pearson's correlation(r) of Atox1-CRIP2 co-localization was calculated by Image Fiji J, at least 20 cells were scored. Scale bar: 10 μm. C) Verification of the Atox1-CRIP2 interaction by streptavidin pull down assay. SA: streptavidin. Relative abundance of Myc-CRIP2 (IP) were quantified and showed in the right panel. Data are shown as means ± s.e.m. and were analyzed by one-way ANOVA comparisons tests. ***$P<0.001$. D) Detection of Atox1 and CRIP2 binding by SPR assay in the presence of Cu^{I}. Purified Atox1 (20 $\mu g\,mL^{-1}$) protein was immobilized on CM5 chip that the final immobilized Atox1 levels were typically ca. 10000 RU. CRIP2 was serially diluted and injected at a flow rate of 30 $\mu L\,min^{-1}$ for 1 min (contact phase) followed by a 1 min (dissociation phase) wash with running buffer supplemented with Cu^{I}. Data are representative of three independent experiments.

a zinc-charged resin, but not to a metal-free control resin (Figure S6F).

The binding of copper to proteins can also be readily monitored using high-resolution ESI-MS.[21] The reaction of Cu^{I} with apo-CRIP2 resulted in a 253.5 Da [4 Cu^{I}] increase in the molecular weight (22827 Da) of the CRIP2 spectrum, thus revealing that Cu^{I} binding is mediated by interactions of as many as four Cu^{I} ions, potentially with multiple CRIP2 regions (Figure 3B). Similar results were observed using UV spectroscopy. UV absorption increased almost linearly with increasing concentrations of Cu^{I} until reaching a plateau at approximately four Cu^{I} equivalents (Figure 3C).

To measure CRIP2's binding affinity for Cu^{I}, we performed a series of ligand competition experiments using bathocuproinedisulfonic acid (BCS),[22] a higher affinity chromogenic chelator that forms a 2:1 complex with Cu^{I} ions. Titration of $Cu(BCS)_2^{3-}$ with apo-CRIP2 revealed a concentration-dependent attenuation of the $Cu(BCS)_2^{3-}$ concentration. Subsequently, we obtained an average Cu^{I} affinity (K_{Cu}) of $1.89\pm0.05\times10^{17}\,M^{-1}$ at pH 7.4 and the overall formation constant of Cu_4CRIP2 ($\log\beta_4=69.11\pm0.05$), which fit well with a model of 4:1 Cu-CRIP2 stoichiometry (Figure 3D and S7A). A Hill plot of Log-(θ/(1-θ)) versus Log [Cu^{I}_{free}] yielded a straight line with a slope (Hill coefficient) of 3.62, indicating cooperative binding between the four Cu^{I} binding sites (Figure S7B). These findings suggest that Cu^{I} binds tightly to CRIP2. No copper binding was detected for the $CRIP2^{CBM}$ mutant (Figure 3D and S7C), supporting that cysteine residues mediate the observed copper binding of $CRIP2^{WT}$.

We also conducted BCS competition assays which revealed a K_{Cu} value of $7.39\pm4.5\times10^{17}\,M^{-1}$ at pH 7.4 and a K_{Cu} value of $3.52\pm1.55\times10^{17}\,M^{-1}$ at pH 7.0 for Atox1's binding affinity with Cu^{I} (Figure S7D-G). Thus, although CRIP2 has a detected Cu^{I} affinity that is slightly weaker than Atox1, the Cu^{I} binding affinities of these two proteins are at the same order of magnitude. This result is not unprecedented: multiple previously studies[23] wherein copper transfer between two proteins does occur despite the Cu^{I} receptor protein having a weaker Cu^{I} binding affinity than the Cu^{I} donor protein (e.g., from Atx1 to PacS and from SenC to PccA). In addition, our SPR assay support that Cu^{I} can promote the interaction

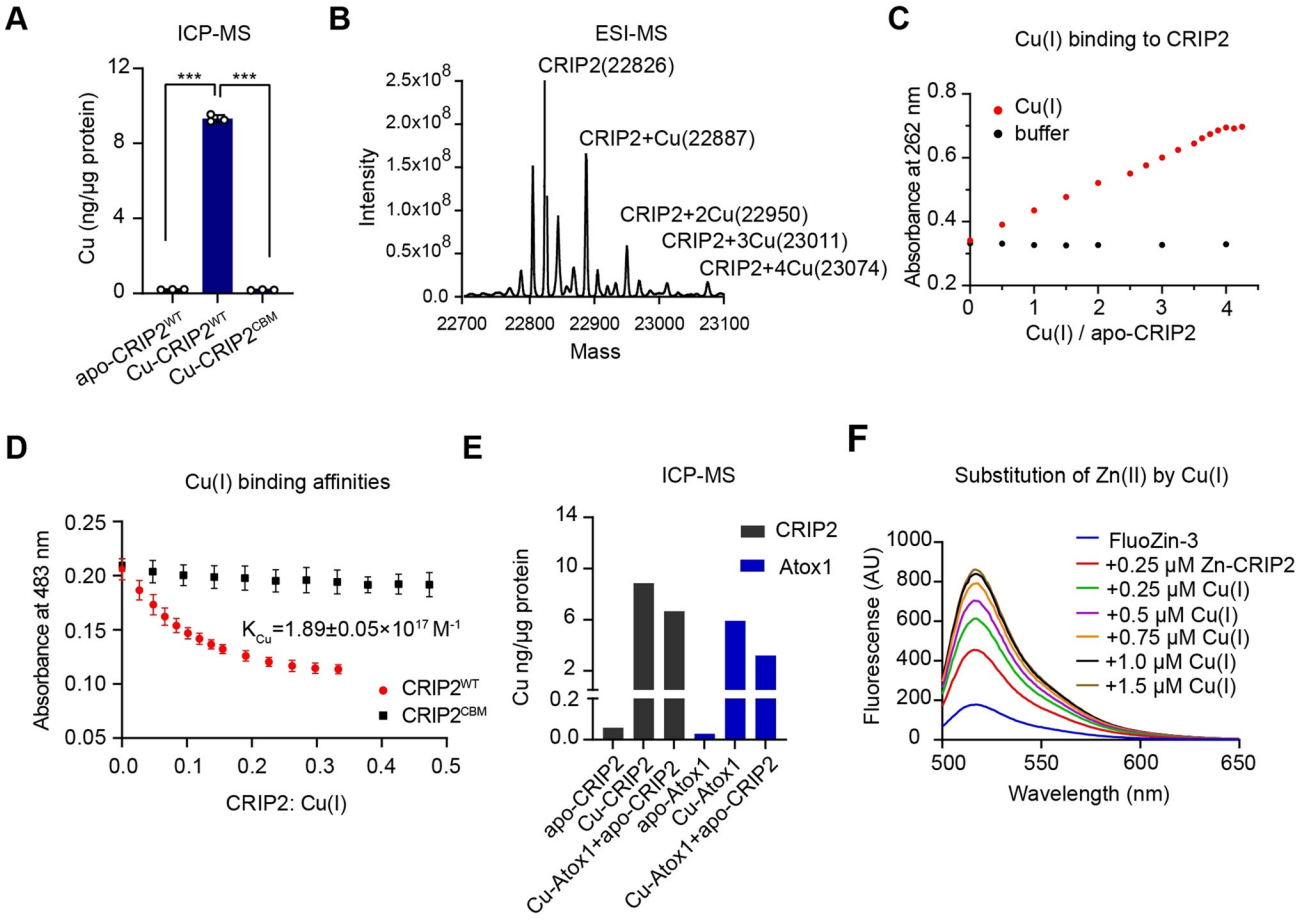

Figure 3. Characterization of Cu^{I} binding to CRIP2. A) ICP-MS quantified the copper-binding capacities of 10 µg purified recombinant $CRIP2^{WT}$ and $CRIP2^{CBM}$ proteins. B) De-convoluted ESI-MS spectra of 10 µM CRIP2 reaction with Cu^{I}. The sample was separated by UPLC followed by ESI-MS analysis. C) UV absorption at 262 nm, measured by adding Cu^{I} to 10 µM apo-CRIP2. D) BCS competition assay to determine Cu^{I} affinities for $CRIP2^{WT}$ and $CRIP2^{CBM}$. Cu^{I} was loaded with 11.7 equivalents of BCS to ensure that all Cu^{I} ligand is found in the chromophoric 1:2 complex with BCS. The $Cu(BCS)_2^{3-}$ solution (Cu^{I}, 16 µM; BCS, 187.5 µM) was then titrated with DTT-free apo-$CRIP2^{WT}$ or $CRIP2^{CBM}$, followed by incubation for 1 min before absorption measurement from 700 nm to 380 nm. Absorption at 483 nm was plotted as a function of the concentration ratio of CRIP2 and Cu^{I}. E) Measurement of copper content of each protein peak in SEC analysis, with ICP-MS. Individual apo- and Cu- forms of both proteins were analyzed after SEC elution. For the mixing experiments, a mixture of Cu-Atox1 and apo-CRIP2 was separated, and both protein peaks were analyzed individually. F) Fluorescence emission spectra of 0.25 µM Zn-CRIP2 with 5 µM FluoZin-3 loaded in 50 mM HEPES at pH 7.4 plus 200 mM NaCl, during titration with Cu^{I}. All data are representative of three independent experiments. Data represent means ± s.e.m. *P* values were determined by one-way ANOVA comparisons tests (A and E). $^{**}P<0.01$, $^{***}P<0.001$.

between Atox1 and CRIP2. Thus, we consider that Cu^{I} transfer can occur between Atox1 and CRIP2.

To investigate the idea of Cu transfer between Atox1 and CRIP2, we took advantage of an observation from our size exclusion chromatography (SEC) analysis which showed that CRIP2 elutes separately from Atox1. Note that SEC has been used previously to probe Cu transfer between two copper-binding proteins;[24] Both the apo- and Cu-form of Atox1 and CRIP2 proteins were separated, and individual fractions were collected to enable ICP-MS based analysis of copper content[24] (Figure S8). The apo-form CRIP2 and Atox1 contained less than 0.1 ng Cu per µg protein (Figure S8A and S8C), while the Cu-form CRIP2 and Atox1 contained 8.85 and 5.91 ng Cu per µg protein (Figure S8B and S8D), respectively. When Cu-Atox1 was mixed with apo-CRIP2, the subsequent SEC elution profiles indicated that Cu^{I} had been transferred from Atox1 to CRIP2: there was a detected decrease in the copper content for the eluted Atox1 as compared to the individually analyzed Cu-Atox1 (from 5.91 to 3.19 ng Cu per µg Atox1) (Figure 3E, S8D-F). Moreover, the eluted CRIP2 had a detected increase in copper content as compared to the individually analyzed apo-CRIP2 (from less than 0.1 to 6.67 ng Cu per µg CRIP2) (Figure 3E, S8A, S8E and S8F). These results indicate that the physical interaction of Atox1 and CRIP2 can support the transfer of copper from Atox1 to CRIP2.

Cu^{I} and Zn^{II} both bind at the same sites of CRIP2, we tested Zn^{II} binding affinities with competition experiments using the Zn^{II} fluorescent indicator FluoZin-3,[25] which is highly sensitive to Zn^{II} but not Cu^{I} (Figure S9A and S9B). We first determined that binding affinity for Zn^{II} of CRIP2 (K_{Zn}) is $(1.47\pm0.46)\times10^{9}\ M^{-1}$, which is much lower than the aforementioned affinity of Cu^{I} and CRIP2 (Figure S9C and S9D). In the presence of FluoZin-3, the addition of Cu^{I} to Zn-

CRIP2 results an increase of FluoZin-3 fluorescence, indicative of Zn^{II} ejection from CRIP2. Importantly, the observed Cu^{I} concentration dependence of the increase in FluoZin-3 fluorescence reached a plateau when Cu^{I} was added at 4:1 molar ratio of Zn-CRIP2 (1:1 molar ratio of metal ions), indicating that the Zn^{II} ions initially bound by CRIP2 can be fully substituted with Cu^{I} ions (Figure 3F). This is consistent with reports for other metalloproteins: although ZF domains have similar Cu^{I}- and Zn^{II}-binding residues, these domains can exhibit considerable variability among their coordination motifs.[2b] Given the greater binding affinity observed for Cu^{I} relative to Zn^{II}, it is probable that Cu^{I} binding substantially alters the ZF structure and potentially its function.

We next investigated the effects of differential Zn^{II} or Cu^{I} binding on the CRIP2 protein conformation. Far-UV CD (190–260 nm) analysis revealed that the binding of zinc did not alter the secondary structure of apo-CRIP2 (Figure S10A and S10B). In contrast, apo-CRIP2′s secondary structure was obviously altered upon binding to copper (Figure S10C and S10D). We next investigated the effect of adding different equivalents of Cu^{I} on the far-UV CD spectra of Zn^{II}-bound CRIP2: the detected change in CRIP2′s secondary structure is similar to the Cu^{I}-loaded form of CRIP2, indicating that Zn trans-chelation by Cu can lead to conformational changes in CRIP2 (Figure S10E and S10F). Notably, we found that the electrophoretic mobility of CRIP2 was altered under the addition of copper, whereas no mobility shifts were observed when the samples included the Cu^{I} specific chelator BCS (Figure S11A); nor were any shifts detected with $CRIP2^{CBM}$ samples (Figure S11B). These results demonstrate a Cu^{I}-binding induced change in CRIP2′s secondary structure.

It has been reported that the stability of several copper-binding proteins is regulated by copper.[2b,26] We monitored the thermal stability of recombinant CRIP2 in the presence of increasing copper/zinc equivalents using the Uncle Uni stability platform. The Tm of CRIP2 decreased as the copper equivalents increased (Figure S11C and S11D); no change in the Tm occurred with increasing zinc (Figure S11E and S11F), suggesting that copper may decrease CRIP2′s stability. We also confirmed that exposure to copper reduced the levels of both endogenous and recombinant CRIP2 in H1299 and HEK293T cells, respectively (Figure 4A and 4B), and this reduction was blocked by co-treatment with the copper chelator BCS (Figure 4C). No copper dependent changes in stability were detected for $CRIP2^{CBM}$ (Figure 4D). We also measured the degradation kinetics of CRIP2 in assays with the translation inhibitor CHX. After 10 h of CHX treatment, the CRIP2 level had decreased by 36% in the control group cells (Figure S12A and S12B); the CRIP2 level was further reduced in the copper-treated cells (a 57% decrease). No additional degradation was detected for $CRIP2^{CBM}$ upon the addition of copper (Figure S12C and S12D). These results together suggest that CRIP2 is relatively more susceptible to degradation in its copper-bound form.

To investigate whether the copper-mediated reduction in CRIP2 protein stability involves the Ubiquitin/Proteasome System (UPS), we conducted assays with the 26S proteasome inhibitor MG132. MG132 significantly reduced the extent of CRIP2 degradation in H1299 cells (Figure 4E). We therefore hypothesized that copper may somehow promote the ubiquitination and proteasomal degradation of CRIP2 in cells. Pursuing this, we co-transfected 3xFlag-tagged CRIP2 and 6xHis-tagged ubiquitin into HEK293T cells with or without copper treatment. We then purified the lysates using nickel chromatography and measured ubiquitinated CRIP2 levels: copper significantly enhanced CRIP2 ubiquitination (Figure 4F). Taken together, these results demonstrating that CRIP2 is relatively more susceptible to degradation in its copper-bound form raise the possibility that a relatively weak elevation in the free copper content in cells could result in pronounced increases in polyubiquitination that prevent cell damage by accelerating protein degradation.

This copper-enhanced ubiquitination and degradation of CRIP2 prompted us to further explore the biological functions of CRIP2. Recent studies established strong links between autophagy and copper-binding proteins:[4c] the copper-binding proteins ULK1/2 are upstream kinases of autophagy, and changes in intracellular copper levels can modulate ULK1/2 kinase activity to affect ULK1/2 dependent autophagy.[27] We generated CRIP2 knockdown cells (KD) with small interfering RNA (siRNAs) (Figure S13A), and immunoblotting revealed that the LC3II signal increased in the CRIP2-knockdown cells compared with scramble control cells (Figure 5A, see also quantification in Figure S13B).

Autophagy is a dynamic process, in which LC3II generation is followed by its degradation in the autolysosome; thus, an increase in LC3II levels can be derived either from de novo autophagy induction or from inhibition of protein degradation by autolysosome.[28] To discriminate between these possibilities, we used Bafilomycin A1 (BafA1), which is a known inhibitor of the late phase of autophagy that prevents the degradation of LC3II by inhibiting fusion between autophagosomes and lysosome.[29] Treatment with BafA1 increased the LC3II level in both scramble control cells and CRIP2-KD cells (Figure 5A and Figure S13B), but the magnitude of the LC3II level increase was substantially greater in CRIP2-KD cells, suggesting that CRIP2 knockdown can somehow increase autophagosome formation rather than the impairment of degradation.

We also found that treatment with the autophagy activator rapamycin enhanced the LC3II level in both control and CRIP2-KD cells (Figure 5B and Figure S13C), with the increase in LC3II more pronounced for the CRIP2-KD cells. Similarly, LC3II levels were substantially increased in CRIP2-knockout (KO) cells (Figure S13D and S13E). Degradation of p62 is another widely used marker to monitor autophagic activity because p62 directly binds to LC3 and is selectively degraded by autophagy.[30] The p62 level was decreased in CRIP2 knockdown cells compared to scramble control cells, further supporting activation of autophagy upon disrupting CRIP2 function (Figure 5B and Figure S13F).

3-methyladenine (3-MA) is a small molecule inhibitor of autophagy that targets the VSP34/PI3K kinase complex.[31] Interruption of autophagy by 3-MA reversed the CRIP2 KD-induced LC3II levels (Figure 5C and Figure S13G). We next examined autophagic flux using GFP-LC3. Compared with control cells, CRIP2-KD cells displayed higher overall

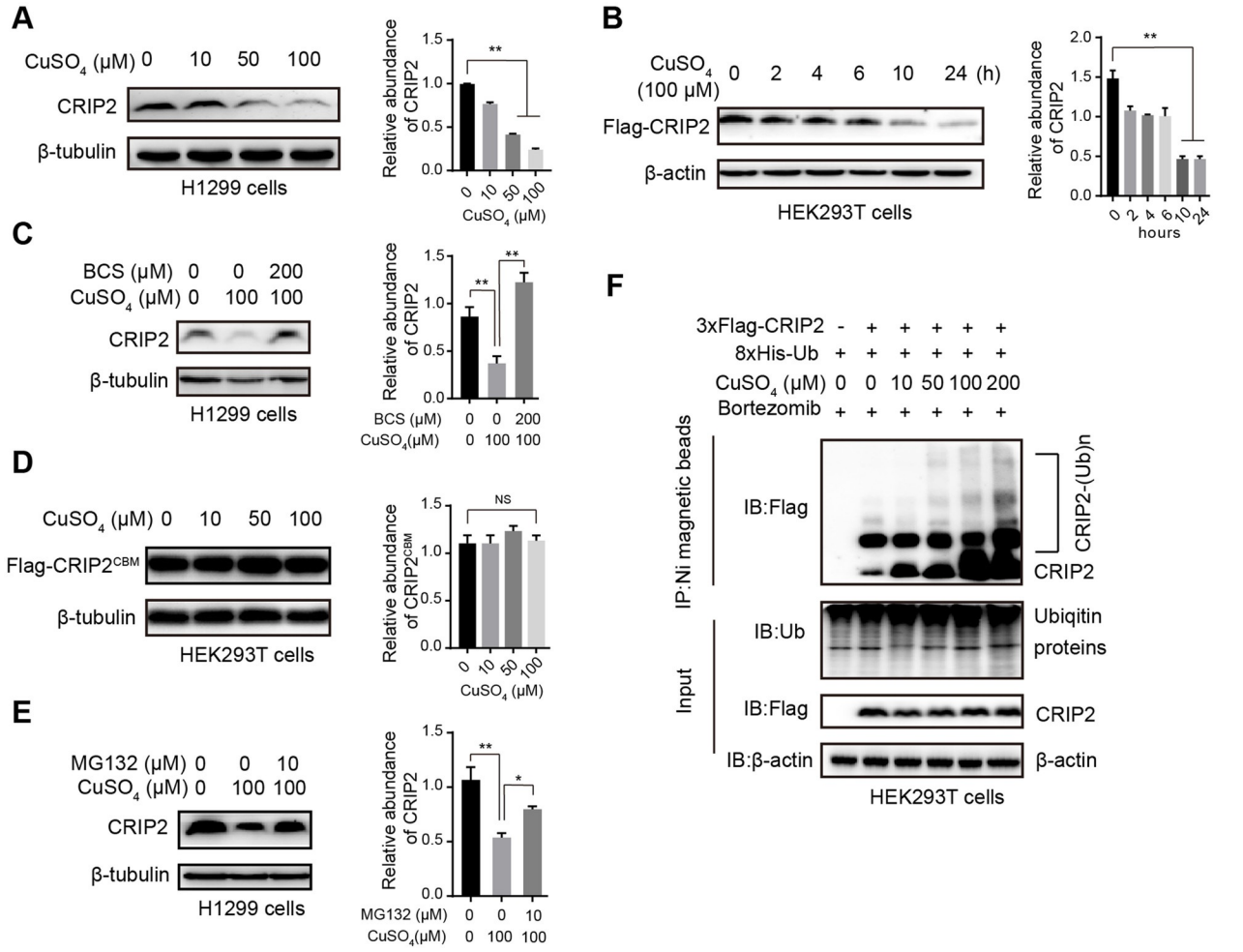

Figure 4. Copper decreases the stability of CRIP2 and promotes its polyubiquitination and subsequent degradation. A) H1299 cells were treated with the indicated concentrations of copper for 24 h, cell lysates were subjected to immunoblotting against CRIP2. B) Immunoblot detection of Flag-CRIP2 in HEK293T cells transfected with Flag-CRIP2 for 36 h, treatment with 100 μM copper for the indicated time. C) Immunoblot detection of CRIP2 under 100 μM copper treatment in the presence or absence of 200 μM BCS in H1299 cells. D) HEK293T cells were transfected with $CRIP2^{CBM}$ for 36 h; after treatment with the indicated concentrations of copper for 24 h, cell lysates were subjected to immunoblotting against Flag. E) Immunoblot detection of CRIP2 from H1299 cells treated with 100 μM copper in the presence or absence of 10 μM MG132 for the last 6 h. F) Copper triggers in vivo polyubiquitination of CRIP2. All data are representative of three independent experiments. The relative abundance of CRIP2 were quantified and showed in the right panel in A, B, C, D and E. Data represent means ± s.e.m. P values were determined by one-way ANOVA comparisons tests. NS: no significance; $*P<0.05$, $**P<0.01$.

abundance of GFP puncta and significantly increased LC3 flux under rapamycin treatment. Importantly, without rapamycin stimulation, CRIP2-KD cells also showed an increased number of bright LC3 puncta compared with control cells (Figure 5D). Similar results were obtained in CRIP2-KO cells (Figure S13H). In addition, electron microscopy (EM) and morphometric analysis revealed numerous autophagy structures in CRIP2-KD cells, in contrast to a scarcity of autophagic structures in control cells (Figure 5E). Taken together, these observations demonstrated that depletion of CRIP2 results in significant activation of autophagy.

We also found that the elevation of LC3II was abrogated upon re-expression of $CRIP2^{WT}$ in CRIP2-KO cells, suggesting that CRIP2 functions as an autophagy suppressor (Figure 6A). To evaluate the effects of disrupting CRIP2 copper binding on autophagy, we re-expressed $CRIP2^{CBM}$ and $CRIP2^{WT}$ in CRIP2-KO cells treated with copper. The LC3II levels increased upon re-expressing $CRIP2^{WT}$ (Figure 6A), indicating that copper promoted the degradation of the re-expressed $CRIP2^{WT}$ and thus promoted autophagy. However, no elevation of LC3II was detected upon re-expression of $CRIP2^{CBM}$ and exposure to copper (Figure 6A), indicating that the copper binding is essential to CRIP2′s function in promoting autophagy. Notably, we also detected that CRIP2-KD and KO cells had increased levels of reactive oxygen species (ROS) (Figure 6B and Figure S13I) and found that the increase in LC3II levels in these cells could be rescued by treatment with the ROS scavenger N-acetyl-L-cysteine (NAC) (Figure 6C). These results are consistent with previous reports showing that ROS signaling is upstream of autophagy activation.[32]

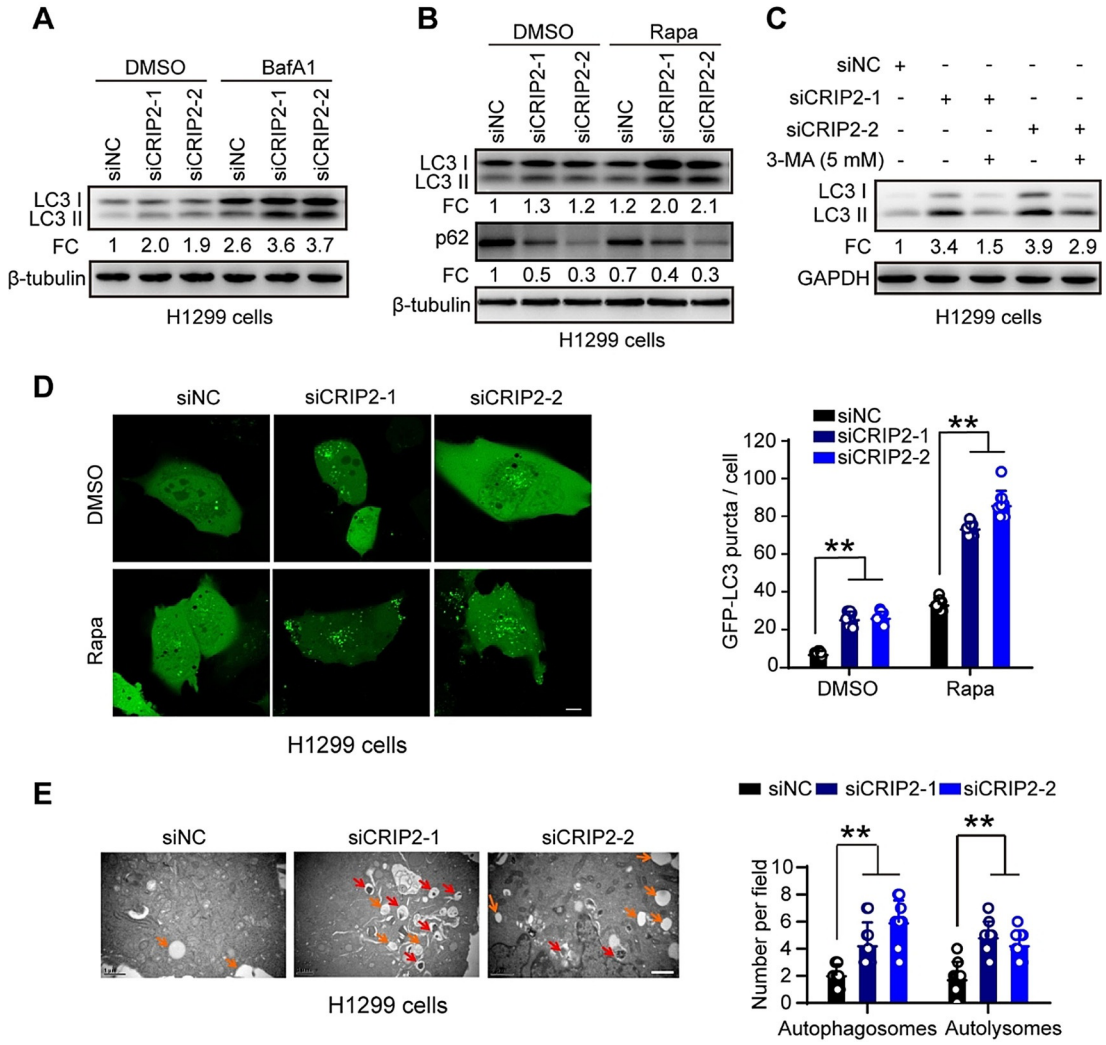

Figure 5. CRIP2 deficiency in H1299 cells enhances autophagic flux. (A–C) Immunoblot detection of LC3I, LC3II or p62 from H1299 cells transfected with CRIP2 siRNA treated with or without BafA1 (20 nM) for 4 h (A); or treated with or without rapamycin (500 nM) for 4 h (B); or treated with or without 3-MA (5 mM) for 24 h (C). FC (fold change): LC3II or p62 levels were quantified relative to β-tubulin/GAPDH and by densitometry using Image J, normalized to the first line. The quantitative data were shown in Figure S11B, 11C, 11F and 11G. D) Fluorescent images of H1299 cells transfected with LC3-EGFP plasmids and then treated with DMSO or Rapamycin (500 nM) for 4 h. Scale bar: 20 μm. Right panel: Mean GFP-LC3 puncta per cell from treated cells ($n=10$, $^{**}P<0.01$). (E) TEM images of siCRIP2 cells. Arrows represent autophagosomes (orange) and autolysomes (red). Scale bar: 1 μm. Right panel: Quantification of autophagosomes and autolysomes. Data are representative of three independent experiments in (A, B and C). Data represent means ± s.e.m. P values were determined by two-way ANOVA followed by Tukey's multiple-comparisons test (D and E). $^{**}P<0.01$.

Conclusion

In this study, we employed a proximity protein labeling strategy to profile proteins that interact with Atox1 in the nucleus of lung cancer cells, seeking to better understand Atox1's connection(s) with tumorigenesis. This approach successfully identified that CRIP2 interacts with Atox1 and functions as a copper-binding protein. There is an extensive literature demonstrating physical interactions between CRIP2 and diverse transcription factors (e.g., *MyoD*, *SRF*, and *GATA* family TFs),[33] and a CRIP2-NF-κB/p65 interaction was previously shown to suppress the transcription of *IL-6*, *IL-8*, and *VEGF*.[19a] As it lacks any obvious DNA-binding homeodomain, the copper-related regulatory impacts of CRIP2 do not apparently result from direct interaction with targeted promoters.

We found that copper-loading promotes ubiquitin-mediated proteasomal degradation of CRIP2, and finally demonstrate that depletion CRIP2 and copper-induced CRIP2 degradation activate autophagy through increased ROS levels in H1299 cells (Figure 6D). Thus, CRIP2 appears to normally function in a negative regulatory role to prevent autophagy activation. Cancer cells are known to accumulate copper, and our findings that CRIP2 is relatively more susceptible to degradation in its copper-bound suggest that cancer cells may selectively discard CRIP2 to protect their viability. These results identify an essential and unrecognized role for a copper-transport-related Atox1-CRIP2 axis in autophagy signaling in lung cancer cells. A better under-

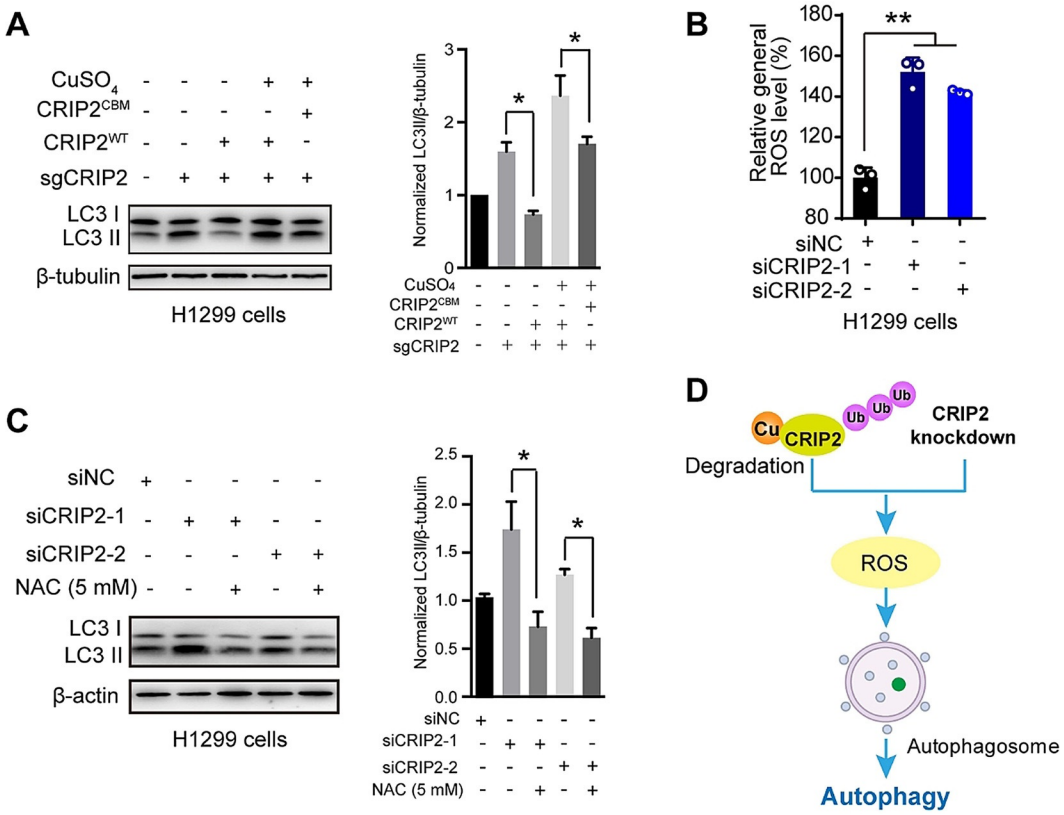

Figure 6. CRIP2 knockdown induced autophagic flux by increasing intracellular ROS. A) Immunoblot detection of LC3I and LC3II from CRIP2 knockout cells transfected with $CRIP2^{WT}$ or $CRIP2^{CBM}$, treated with or without $CuSO_4$ (100 μM) for 12 h. Right panel: Quantification of LC3-II/β-tubulin normalized to the band of the first lane. B) ROS levels were detected with DCFH-DA and analyzed by FACS in CRIP2-depleted H1299 cells. C) Immunoblot detection of LC3I and LC3II from CRIP2-depleted H1299 cells treated with 5 mM NAC for 12 h. Right panel: Quantification of LC3-II/β-actin normalized to siNC. D) Proposed model for the regulatory pathway in CRIP2 knockdown cells. Data are representative of three independent experiments (A, B and C). Data represent means ± s.e.m. P values were determined by one-way ANOVA comparisons tests (A, B, and C). $*P<0.5$, $**P<0.01$.

standing of how copper trafficking from copper chaperones to copper-binding proteins is dynamically regulated in response to changing cellular requirements could support the development of improved therapies for disorders involving dysregulated copper metabolism.

Cu^{I} exhibits high affinity for thiolate ligands, suggesting that thiol-rich zinc binding sites may be subject to disruption during copper stress conditions. The presence of multiple CXXC repeats in CRIP2 support a capacity for Cu^{I} to interact with these motifs, and we confirmed that CRIP2 directly binds with copper, with an average binding affinity ($10^{17}\ M^{-1}$) higher than for zinc ($10^{9}\ M^{-1}$). Cu/Zn competition assays also confirmed that Cu^{I} ions are able to substitute Zn^{II} in CRIP2, and our circular dichroism (CD) results confirmed that CRIP2 can bind multiple Cu^{I} ions at the Zn^{II} binding sites. The CD analysis also revealed that copper binding induces alteration of CRIP2′s secondary structure. These results suggest a potentially interesting implication, pointing towards a role for CRIP2 at the intersection of Zn^{II} and Cu^{I} trafficking and regulation.

Prior to the present study, bioinformatics and yeast two-hybrid studies had identified a total of seven copper-binding proteins in the nucleus.[11a] The data from our APEX2 screening represents therefore a substantially scope-widening resource for the study of Atox1 in the nucleus, and indicates that the copper transport network extends well beyond what is currently known. Based on quantitative scoring, we will further identify and investigate the biological functions of the remaining Atox1-interacting proteins, starting with those predicted as most likely to bind copper. Finally, we also anticipate that similar proximity labeling approaches to the one we have illustrated in the present study should be generally applicable to other copper chaperones and copper-binding proteins and can be harnessed to map diverse metalloprotein interactions in cells.

Acknowledgements

The authors are grateful to Ting Han, Xiangbin Qi (National Institute of Biological Sciences) and Junli Liu (Shanghai Jiao Tong University) for helpful discussion, and Dr. Xiaohui Zhang and Dr. Yuan Wang for spectroscopic assistance. The authors thank the mass spectrometry facility of National Center for Protein Sciences at Peking University for assistance with the proteomic analysis. This work supported by the National Basic Research Foundation of China (No. 2017YFA0505202 to Jing Wang), the National Natural

Science Foundation of China (21672014 and 91853107 to Jing Wang).

Conflict of Interest

The authors declare no conflict of interest.

Keywords: Atox1 · autophagy · copper · cysteine-rich protein 2 (CRIP2) · engineered ascorbate peroxidase (APEX2)

[1] a) R. A. Festa, D. J. Thiele, *Curr. Biol.* **2011**, *21*, R877 – R883; b) L. A. Finney, T. V. O'Halloran, *Science* **2003**, *300*, 931 – 936; c) V. Culotta, *J. Biol. Inorg. Chem.* **2010**, *15*, 1 – 2; d) S. Lutsenko, N. L. Barnes, M. Y. Bartee, O. Y. Dmitriev, *Physiol. Rev.* **2007**, *87*, 1011 – 1046.

[2] a) R. T. Doku, G. Park, K. E. Wheeler, K. E. Splan, *J. Biol. Inorg. Chem.* **2013**, *18*, 669 – 678; b) A. R. Mufti, E. Burstein, R. A. Csomos, P. C. F. Graf, J. C. Wilkinson, R. D. Dick, M. Challa, J. K. Son, S. B. Bratton, G. L. Su, G. J. Brewer, U. Jakob, C. S. Duckett, *Mol. Cell* **2006**, *21*, 775 – 785; c) B. Prasser, L. Schöner, L. Zhang, O. Einsle, *Angew. Chem. Int. Ed.* **2021**, *60*, 18810 – 18814; *Angew. Chem.* **2021**, *133*, 18958 – 1896.

[3] R. J. Coates, N. S. Weiss, J. R. Daling, R. L. Rettmer, G. R. Warnick, *Cancer Res.* **1989**, *49*, 4353 – 4356.

[4] a) D. C. Brady, M. S. Crowe, M. L. Turski, G. A. Hobbs, X. J. Yao, A. Chaikuad, S. Knapp, K. H. Xiao, S. L. Campbell, D. J. Thiele, C. M. Counter, *Nature* **2014**, *509*, 492 – 496; b) L. Krishnamoorthy, J. A. Cotruvo, Jr., J. Chan, H. Kaluarachchi, A. Muchenditsi, V. S. Pendyala, S. Jia, A. T. Aron, C. M. Ackerman, M. N. Wal, T. Guan, L. P. Smaga, S. L. Farhi, E. J. New, S. Lutsenko, C. J. Chang, *Nat. Chem. Biol.* **2016**, *12*, 586 – 592; c) E. V. Polishchuk, A. Merolla, J. Lichtmannegger, A. Romano, A. Indrieri, E. Y. Ilyechova, M. Concilli, R. De Cegli, R. Crispino, M. Mariniello, R. Petruzzelli, G. Ranucci, R. Iorio, F. Pietrocola, C. Einer, S. Borchard, A. Zibert, H. H. Schmidt, E. Di Schiavi, L. V. Puchkova, B. Franco, G. Kroemer, H. Zischka, R. S. Polishchuk, *Gastroenterology* **2019**, *156*, 1173 – 1189 e1175; d) M. L. Turski, D. C. Brady, H. J. Kim, B. E. Kim, Y. Nose, C. M. Counter, D. R. Winge, D. J. Thiele, *Mol. Cell. Biol.* **2012**, *32*, 1284 – 1295.

[5] Y. Liao, J. J. Zhao, K. Bulek, F. Q. Tang, X. Chen, G. Cai, S. Jia, P. L. Fox, E. Huang, T. T. Pizarro, M. F. Kalady, M. W. Jackson, S. D. Bao, G. C. Sen, G. R. Stark, C. J. Chang, X. X. Li, *Nat. Commun.* **2020**, *11*, 900.

[6] a) A. Gupte, R. J. Mumper, *Cancer Treat. Rev.* **2009**, *35*, 32 – 46; b) D. Denoyer, S. Masaldan, S. La Fontaine, M. A. Cater, *Metallomics* **2015**, *7*, 1459 – 1476.

[7] I. Hamza, A. Faisst, J. Prohaska, J. Chen, P. Gruss, J. D. Gitlin, *Proc. Natl. Acad. Sci. USA* **2001**, *98*, 6848 – 6852.

[8] V. Shanbhag, K. Jasmer-McDonald, S. Zhu, A. L. Martin, N. Gudekar, A. Khan, E. Ladomersky, K. Singh, G. A. Weisman, M. J. Petris, *Proc. Natl. Acad. Sci. USA* **2019**, *116*, 6836 – 6841.

[9] S. Itoh, H. W. Kim, O. Nakagawa, K. Ozumi, S. M. Lessner, H. Aoki, K. Akram, R. D. McKinney, M. Ushio-Fukai, T. Fukai, *J. Biol. Chem.* **2008**, *283*, 9157 – 9167.

[10] a) D. L. Huffman, T. V. O'Halloran, *Annu Rev Biochem.* **2001**, *70*, 677 – 701; b) C. H. Yu, N. Yang, J. Bothe, M. Tonelli, S. Nokhrin, N. V. Dolgova, L. Braiterman, S. Lutsenko, O. Y. Dmitriev, *J. Biol. Chem.* **2017**, *292*, 18169 – 18177.

[11] a) H. Öhrvik, P. Wittung-Stafshede, *Int. J. Mol. Sci.* **2015**, *16*, 16728 – 16739; b) M. Matson Dzebo, S. Blockhuys, S. Valenzuela, E. Celauro, E. K. Esbjorner, P. Wittung-Stafshede, *Comput. Struct. Biotechnol. J.* **2018**, *16*, 443 – 449.

[12] a) S. S. Lam, J. D. Martell, K. J. Kamer, T. J. Deerinck, M. H. Ellisman, V. K. Mootha, A. Y. Ting, *Nat. Methods* **2015**, *12*, 51 – 54; b) J. Paek, M. Kalocsay, D. P. Staus, L. Wingler, R. Pascolutti, J. A. Paulo, S. P. Gygi, A. C. Kruse, *Cell* **2017**, *169*, 338 – 349 e311.

[13] Y. Hatori, S. Lutsenko, *Antioxid. Redox Signaling* **2013**, *19*, 945 – 957.

[14] P. J. Boersema, R. Raijmakers, S. Lemeer, S. Mohammed, A. J. Heck, *Nat. Protoc.* **2009**, *4*, 484 – 494.

[15] A. K. Boal, A. C. Rosenzweig, *Chem. Rev.* **2009**, *109*, 4760 – 4779.

[16] M. Yoneyama, A. Sasagawa, T. Tomizawa, N. Tochio, S. Koshiba, M. Inoue, T. Kigawa, S. Yokoyama. *PDB(2CU8)* in the RCSB protein data bank. **2005** unpublished.

[17] M. A. Karim, K. Ohta, M. Egashira, Y. Jinno, N. Niikawa, I. Matsuda, Y. Indo, *Genomics* **1996**, *31*, 167 – 176.

[18] a) Y. Liang, P. M. Ewing, W. J. Laursen, V. T. Tripp, S. Singh, K. E. Splan, *J. Inorg. Biochem.* **2014**, *140*, 104 – 110; b) A. Badarau, C. Dennison, *Proc. Natl. Acad. Sci. USA* **2011**, *108*, 13007 – 13012.

[19] a) A. K. Cheung, J. M. Ko, H. L. Lung, K. W. Chan, E. J. Stanbridge, E. Zabarovsky, T. Tokino, L. Kashima, T. Suzuki, D. L. Kwong, D. Chua, S. W. Tsao, M. L. Lung, *Proc. Natl. Acad. Sci. USA* **2011**, *108*, 8390 – 8395; b) P. H. Lo, J. M. Ko, Z. Y. Yu, S. Law, L. D. Wang, J. L. Li, G. Srivastava, S. W. Tsao, E. J. Stanbridge, M. L. Lung, *Cancer Lett.* **2012**, *316*, 39 – 45; c) L. Zhou, Y. Wang, M. Zhou, Y. Zhang, P. Wang, X. Li, J. Yang, H. Wang, Z. Ding, *Nat. Commun.* **2018**, *9*, 1480.

[20] F. Hussain, A. Rodriguez-Granillo, P. Wittung-Stafshede, *J. Am. Chem. Soc.* **2009**, *131*, 16371 – 16373.

[21] T. Fang, W. Chen, Y. Sheng, S. Yuan, Q. Tang, G. Li, G. Huang, J. Su, X. Zhang, J. Zang, Y. Liu, *Nat. Commun.* **2019**, *10*, 186.

[22] a) Z. Xiao, A. G. Wedd, *Nat. Prod. Rep.* **2010**, *27*, 768 – 789; b) Z. Xiao, J. Brose, S. Schimo, S. M. Ackland, S. La Fontaine, A. G. Wedd, *J. Biol. Chem.* **2011**, *286*, 11047 – 11055.

[23] a) See Ref. [18b]; b) P. I. Trasnea, A. Andrei, D. Marckmann, M. Utz, B. Khalfaoui-Hassani, N. Selamoglu, F. Daldal, H. G. Koch, *ACS Chem. Biol.* **2018**, *13*, 1388 – 1397.

[24] a) S. Petzoldt, D. Kahra, M. Kovermann, A. P. Dingeldein, M. S. Niemiec, J. Aden, P. Wittung-Stafshede, *Biometals* **2015**, *28*, 577 – 585; b) Z. Xiao, A. G. Wedd, *Chem. Commun.* **2002**, 588 – 589.

[25] M. J. Devinney II, I. J. Reynolds, K. E. Dineley, *Cell Calcium* **2005**, *37*, 225 – 232.

[26] G. F. Brady, S. Galban, X. Liu, V. Basrur, J. D. Gitlin, K. S. Elenitoba-Johnson, T. E. Wilson, C. S. Duckett, *Mol. Cell. Biol.* **2010**, *30*, 1923 – 1936.

[27] T. Tsang, J. M. Posimo, A. A. Gudiel, M. Cicchini, D. M. Feldser, D. C. Brady, *Nat. Cell Biol.* **2020**, *22*, 412 – 424.

[28] S. R. Yoshii, N. Mizushima, *Int. J. Mol. Sci.* **2017**, *18*, 1865.

[29] A. Yamamoto, Y. Tagawa, T. Yoshimori, Y. Moriyama, R. Masaki, Y. Tashiro, *Cell Struct. Funct.* **1998**, *23*, 33 – 42.

[30] G. Bjørkøy, T. Lamark, S. Pankiv, A. Øvervatn, A. Brech, T. Johansen, *Methods Enzymol.* **2009**, *452*, 181 – 197.

[31] Y. Wu, X. Wang, H. Guo, B. Zhang, X. B. Zhang, Z. J. Shi, L. Yu, *Autophagy* **2013**, *9*, 595 – 603.

[32] R. Scherz-Shouval, Z. Elazar, *Trends Biochem. Sci.* **2011**, *36*, 30 – 38.

[33] a) Y. Kong, M. J. Flick, A. J. Kudla, S. F. Konieczny, *Mol. Cell. Biol.* **1997**, *17*, 4750 – 4760; b) D. F. Chang, N. S. Belaguli, D. Iyer, W. B. Roberts, S. P. Wu, X. R. Dong, J. G. Marx, M. S. Moore, M. C. Beckerle, M. W. Majesky, R. J. Schwartz, *Dev. Cell* **2003**, *4*, 107 – 118.

Manuscript received: July 6, 2021
Revised manuscript received: August 25, 2021
Accepted manuscript online: September 22, 2021
Version of record online: October 27, 2021

